# Estudio de la emisión acústica de la fractura de rocas basálticas en ensayo de compresión uniaxial

## *Study of the acoustic emission of basaltic rock fracture in uniaxial compression test*

Alejandra Vesga-Ramírez[1,2], Dino Filipussi[1,3], Emilio Camilión[4] & Martín Gómez[1,2]

**Resumen** La emisión acústica (EA) es un fenómeno útil para estudiar materiales estructurales bajo condiciones de carga variables. A partir de vincular el comportamiento mecánico y algunos parámetros de la EA se puede obtener información sobre los procesos de nucleación y crecimiento de fisuras. En el monitoreo de estructuras volcánicas es de interés el estudio de las ondas elásticas generadas por la fractura de rocas. En este trabajo se realizaron ensayos de compresión uniaxial hasta la rotura en rocas basálticas extraídas del volcán Peteroa de Argentina y se registró la EA generada con el objetivo de comprender los mecanismos de fractura y obtener parámetros indicadores que permitan interpretar la dinámica de las fallas en rocas, en muchos casos por compresión. La carga, controlada por desplazamiento, fue aplicada por etapas de aumento lineal y otras de carga constante en función del tiempo. La amplitud y también los hits, las cuentas y la energía acumulada fueron los parámetros más representativos para evaluar el avance del daño en la roca. El modo de fractura predominante durante cada etapa de carga se midió mediante un método gráfico que vincula la FM y el valor RA. En las etapas iniciales de carga el modo predominante de fractura fue el ténsil, mientras que en la última etapa aumentó la cantidad de señales provenientes de fracturas de tipo corte. También se calculó el valor b-value, el cual fue disminuyendo mientras el daño y la energía de la EA aumentaban. Los resultados obtenidos permiten una caracterización a tiempo real del avance del daño de la roca.

**Palabras clave** Emisión acústica, basalto, volcán Peteroa, fractura tipo tensil, fractura tipo corte.

***Abstract*** *Acoustic emission (AE) is a useful phenomenon to study structural materials under varying loading conditions. By linking mechanical behavior with certain AE parameters, information about nucleation processes and crack growth can be obtained. In the monitoring of volcanic structures, the study of elastic waves generated by rock fracture is of interest. In this work, uniaxial compression tests were carried out until rupture in basaltic rocks extracted from the Peteroa volcano in Argentina, and the generated AE was recorded with the aim of understanding the fracture mechanisms and obtaining indicator parameters that allow interpreting the dynamics of rock faults, often under compression. The load, controlled by displacement, was applied in stages of linear increase and others of constant load as a function of time. The amplitude, hits, counts, and accumulated energy were the most representative parameters to evaluate the damage progress in the rock. The predominant fracture mode during each loading stage was measured by a graphical method linking the FM and the RA value. It was calculated that in the initial stages, the predominant mode was tensile, while in the last stage, the number of signals from shear cracks was higher. The b-value was also calculated and found to decrease as the damage and AE energy increased. The results obtained allow a real-time characterization of the rock damage progress.*

***Keywords*** *Acoustic emission, basalt, Peteroa volcano, tensile crack, shear crack.*

[1]Grupo de Ondas Elásticas, ICES, Centro Atómico Constituyentes, CNEA, Argentina. Email: alejandravesga@cnea.gov.ar
[2]Grupo de Emisión Acústica, FRD, Universidad Tecnológica Nacional, Argentina.
[3]Departamento de Física, ECyT-UNSAM, Universidad Nacional de San Martín, Argentina.
[4]YPF-Tecnología, Berisso, Argentina.

 

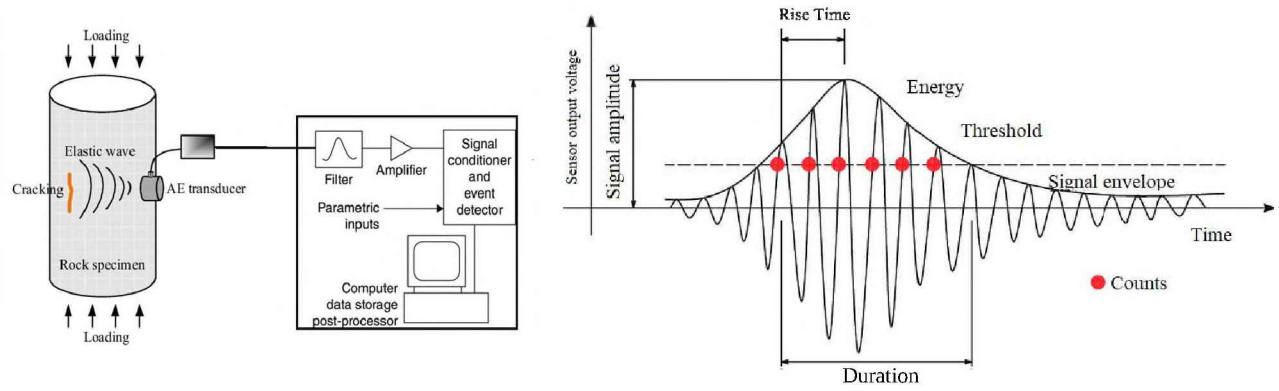


***Figure 1.*** *Acoustic Emission detection principle and typical parameters of the received AE signal.*

## INTRODUCTION

Acoustic Emission (AE) is a widely studied phenomenon that occurs when a material releases energy in the form of elastic waves in response to a stimulus (Ono, 2011; Calabrese & Proverbio, 2020; Casals et al., 2021). These waves, generated by an AE source, can be attributed to microfracture formation, fracture reactivation, fracture propagation, among other processes (Carrasco et al., 2021; Zhao et al., 2022; Li et al., 2022; Niu et al., 2023). Various studies utilizing AE have enhanced our understanding of the formation, growth, and prediction of damage in a variety of materials and rocks (Rodríguez & Celestino, 2019; Zhang et al., 2021; Dong et al., 2023; Cao et al., 2023). Furthermore, advancements in AE research have led to the application of this technique in additional research areas. Recently, AE detection has been employed to analyze fractures induced by changes in fluid pressure in pores and fluid injection (Wu et al., 2022; Shi et al., 2023). These findings have expanded the possibilities of AE and provided new insights into material responses to different loading stress.

Most AE studies are concerned with analyzing rock fracture under a single stressed state (Wieser et al., 2015; Wang et al., 2019). However, in practical engineering scenarios, rocks frequently undergo complex stress conditions. The aim of this work is to advance towards a better understanding of fracture mechanisms and failures prediction by investigating the mechanical characteristics and properties of Acoustic Emission (AE) sources in rocks subjected to compression tests under varying load conditions. The resulting failure model from such complexity plays a pivotal role. This knowledge is particularly relevant in areas where surrounding rocks to critical geological and geotechnical structures, such as mountain tunnels, oil well walls, or volcanoes, are subjected to different stress conditions.

## THEORETICAL FOUNDATIONS

### Principle of Acoustic Emission detection

To detect AE, sensors or transducers are used, placed on the surface of the material to be inspected. These devices are designed to capture the elastic waves generated by the material during its normal operation or when subjected to loads or changes in its state. These waves are converted into an electrical signal by the sensor, amplified by the preamplifier, and transmitted to a computer for processing and recording, as shown in Figure 1.

Among the primary features of AE are the Amplitude (A), expressed in dB, indicating the maximum magnitude reached by the AE signal; the Rise Time (RT), in microseconds, representing the time at which occurs that Amplitude and the “energy”, in voltage-time units, defined as the measured area under the rectified AE signal envelope (MARSE). Also, secondary parameters such as the RA value (RA), describing the ratio between RT and Amplitud, as the inverse of the slope at which the maximum amplitude is reached from the beginning of the event; and the Average Frequency (AF), representing

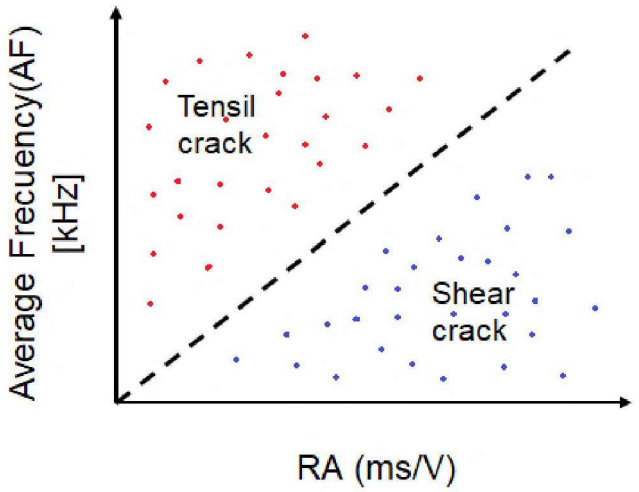


***Figure 2.*** *Schematic diagram of the mean frequency (AF) vs. RA graph for discriminating tensile and shear fractures.*

a mean frequency value of the acoustic waves generated during the event. Additionally, the event duration, indicating the time interval during which the acoustic waves were detected, total released energy, counts, among other parameters, are recorded.

**Classification of fracture modes based on AE**

The classification of AE events plays a crucial role in the analysis of this phenomenon. A commonly used technique for classifying these events is based on the AF vs RA graph (Jiao, 2019; Wang, 2021). Typically, tensile mode fracture AE signals have higher amplitude and shorter rise time than shear fracture signals. Furthermore, the AE average frequency is higher in tensile mode than in shear mode.

The RA value (RA) parameter is obtained from the ratio of Rise Time divided by the Amplitude:

$$RA = \frac{RiseTime\,[ms]}{Amplitude\,[V]} = \text{units} \in ms/V. \tag{1}$$

The Average Frequency (AF) parameter is obtained from the ratio of Counts/Duration:

$$AF = \frac{Counts}{Duration\,[ms]} = \text{units} \in kHz. \tag{2}$$

The AF vs RA graph is a visual representation that allows the evaluation and differentiation of different fracture modes in AE events. In this graph, AE events are represented by dots as depicted in Figure 2.

By interpreting the position of points on the graph, it is possible to classify events into different fracture categories. For example, in Figure 2, events located in a region of the graph, with a high AF ratio and a relatively low RA value, typically correspond to tensile fracture events. On the other hand, events situated in a region with a low AF and a high RA could be associated with shear fracture events.

**b-value**

In the field of seismology, the Gutenberg-Richter law (1954) establishes a relationship between seismic signals of magnitude $A$ and the cumulative number of seismic events $N$ with amplitudes equal to or greater than $A$ (Filipussi, 2018). This relationship follows a potential-type dependency pattern:

$$N = C \cdot A^{-b} \tag{3}$$

And is usually expressed on a logarithmic-logarithmic scales as:

$$\log N = a - b \cdot \log A \tag{4}$$

This relationship is presented as a linear function, where $a$ and $b$ are constants. The exponent $b$ (b-value) represents the relative proportion of fracture events of different sizes advancing during material damage and corresponds to the slope in this linear relationship.

In the context of our AE signal analysis, $N$ represents the cumulative number of AE events with amplitudes greater than or equal to $A$ (Shi, 2023). Data acquisition from the AE equipment plate is described by the following relationship:

$$A_{dB} = 20 \cdot \log\left(\frac{A}{A_0}\right) \tag{5}$$

where $A_{dB}$ is the amplitude measured in decibels; $A$ is the amplitude measured in volts at the output of the piezoelectric sensor (without signal amplification) and $A_0 = 1\ \mu V$ is the reference unit of amplitude. Finally, by replacing Eq. 5 into Eq. 4, the expression used in this work is:

$$\log N = a - b \cdot \left(\frac{A_{dB}}{20}\right) \tag{6}$$

The discernible shifts in b-values are considered to condense crucial precursor information, offering valuable insights into the intricate dynamics of seismic activity. This analytical approach has found widespread application in the exploration of the intricate relationship between seismic magnitude and frequency within the realm of seismology. Anomalous variations in b-values could be a key tool for unraveling the nuanced patterns and predictive cues associated with seismic events, enhancing our understanding of the behavior of the fracture process, and contributing to the advancement of earthquake prediction methodologies. Hence, examining the fluctuation of b-values within AE signals is essential to grasp the underlying mechanisms behind the evolution of the rock damage (Rao & Lakshmi, 2006; Xie et al., 2023).

## METHODOLOGY

Simple uniaxial compression tests were performed to three basalt rock specimens from the Peteroa volcano (Argentina). Specimen dimension of this tests was 89.94 mm in length and 37.93 mm in diameter. The load was applied with a servo hydraulic mechanical testing machine with a maximum load capacity of 440 kN. The tests were performed until specimen failure. Data recorded in this study were acquired using a two-channel Physical Acoustic Corporation AE equipment. The AE parameters were measured during loading process. AE signals were conditioned with a 40 dB preamplifier and filtered through a 20 kHz high-pass filter and a 1 MHz low-pass filter. Two WD PAC sensors were used. The sampling rate was 5 Msamples per second. The detection threshold was set at a value of 42 dB to reject the ambient noise. Digital signal parameters and data were continuously stored in the PC based AE System for subsequent processing. The schematic diagram and photos of the acquisition system are illustrated in Figure 3.

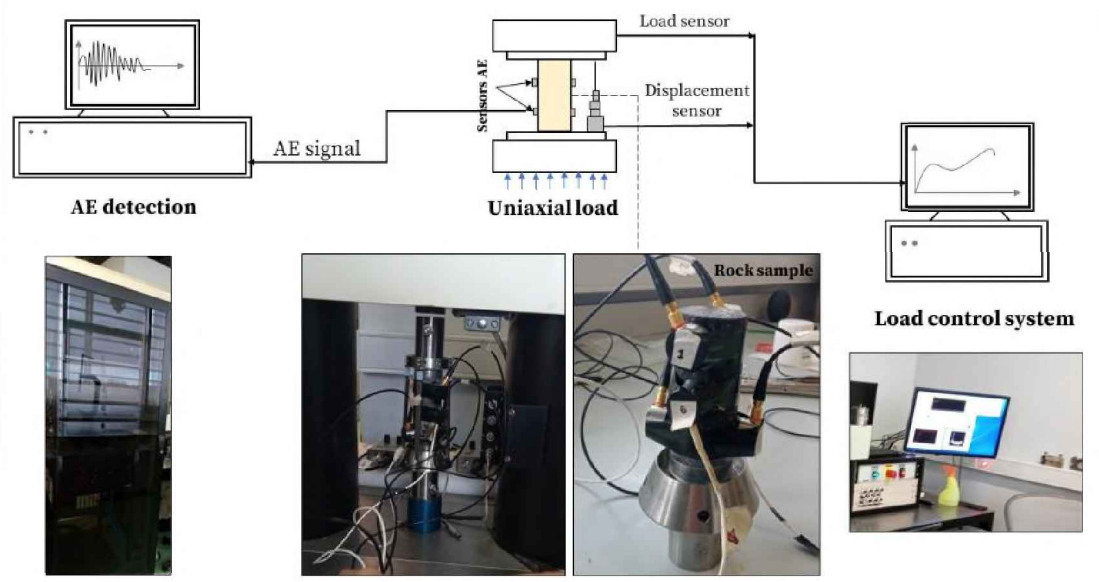


***Figure 3.*** *Experimental design for Acoustic Emission signal acquisition during uniaxial load-controlled rock fracture test.*

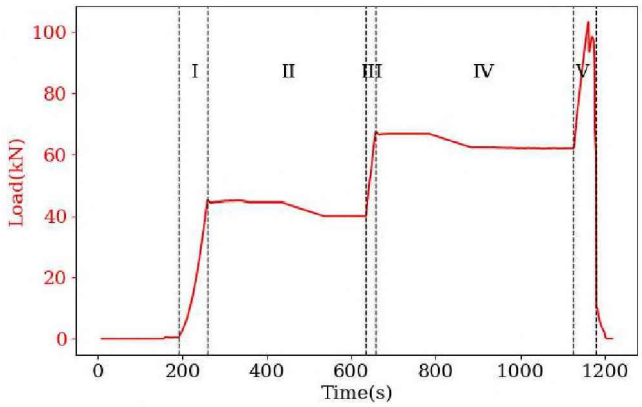


***Figure 4.*** *AE amplitude and load stages during the compression test.*

## Staged division of the test

The load evolution was programmed as five clearly defined stages, depicted in Figure 4. Initially, the load was incrementally raised until reaching 45.5 kN, Subsequently, the second stage maintained a constant load and decrease until 40.6 kN. The third stage witnessed a load transition from 40.6 kN to 67.4 kN. Following this in the four stages, the load was once again held constant until 790s and decrease until 61.8 kN. Finally, in the fifth stage, the load escalated from 61.8 kN to 103.5 kN, marking the point at which specimen fracture occurred. Throughout each of these stages, constant loading between positive slope loading steps was performed to monitor the damage evolution across different stress levels.

## RESULTS

The results presented herein showcase the outcomes of testing for one of the three specimens. These results are consistently replicated for all specimens tested and measured across both channels. AE waveforms and parameters were re-processed by AE Win software. To avoid the ambient noise the AE signals were refiltered with an amplitude threshold of 50 dB. Also, parametric filters for Energy, and Rise Time were applied. Then 2749 hits of AE were identified for both channels during the experiment.

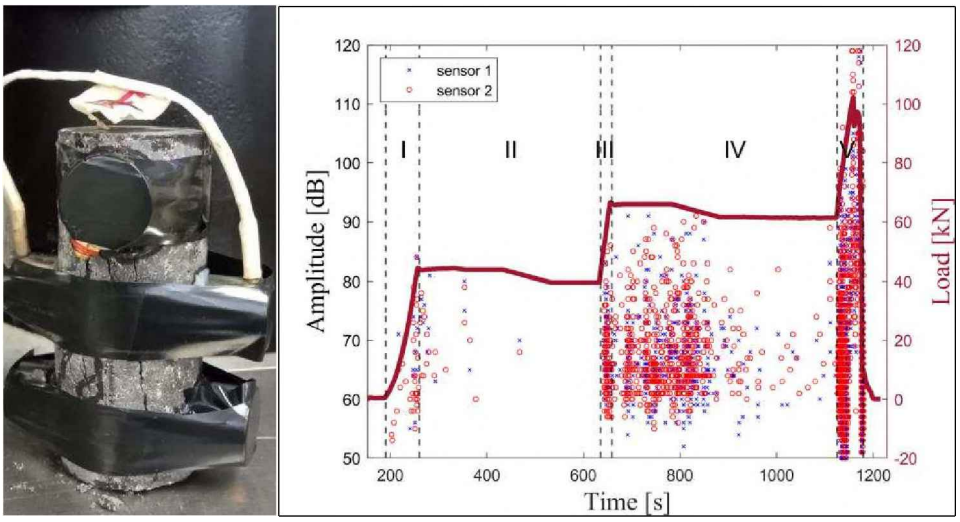


***Figure 5.*** *Applied load on the rock (red line) and amplitude of AE hits (blue and red markers) recorded during the test over time.*

In the following section an analysis of the most representative AE parameters will be presented. These parameters were selected for their ability to show indications when the fracture of the rock sample evolves until rupture during the test.

### Amplitude

This parameter refers to the maximum amplitude value of the AE signal for each hit, represented in dB. Figure 5 displays the recorded amplitudes at each sensor for each detected AE event. The highest amplitude occurred at the time of unstable crack propagation coinciding with the maximum applied load. By overlaying in the graph of Figure 5 the applied load on the specimen and the amplitude of AE hits, it can be observed how the occurrence and amplitude of AE hits increases in correlation with the load increment (stage I, III, V). Similarly, in the same graph, a decrease in the number of the recorded AE hits is observed when the load remains constant (stage II and IV).

### Accumulated hits vs time

The hit occurrence time ("hit time") refers to the moment when an AE event is deemed to commence. This happens when the signal of each hit first surpasses the threshold. Figure 6 illustrates the accumulated hits (the cumulative sum of hits over time) from both acquisition channels, demonstrating their correlation with applied load. It can be observed that towards the end of stage I, there is a rise in hits, causing a slight elevation in the slope of accumulated hits. However, as the load remains constant in stage II, the hits remain steady. Only in stage III, when the load reaches 60%, do the hits begin to increase, indicating that considerable damage to the specimen may occur beyond 40%. In stage IV, the hits continue to grow if the load remains constant; however, if the load decreases, as observed around 900 s, the accumulated hits cease to increase, suggesting susceptibility to damage occurs around 60%. This is consistent with stage V, where the load returns to 60%, and the accumulated hits spike, reaching their maximum peak near the load's maximum peak and the total fracture of the samples rocks.

Counts The parameter "counts" denotes the frequency of signal amplitudes exceeding a predefined voltage threshold for each AE hit. On the left side of Fig. 7, the count of occurrences recorded for each AE channel is observed throughout the test duration. On the right side of Figure 7, the cumulative count is depicted, overlaying the applied load curve during the test. During stages I and II, the cumulative counts remain at a constant and low value. In stage III, a significant increase in the slope of cumulative counts is evident, signifying the onset of damage for the first time to the specimens. In stage IV,

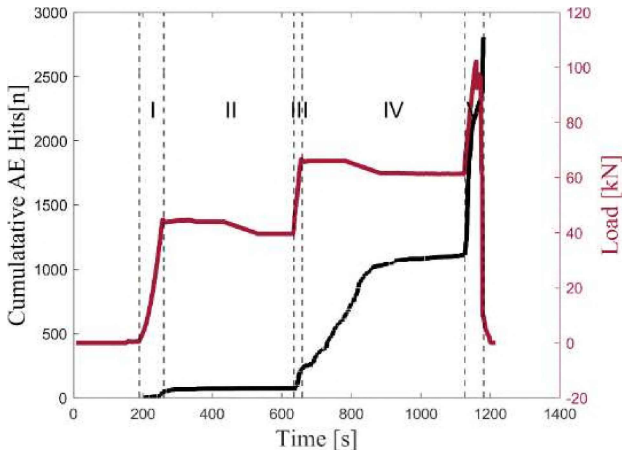


***Figure 6.*** *AE cumulative hits and load vs time.*

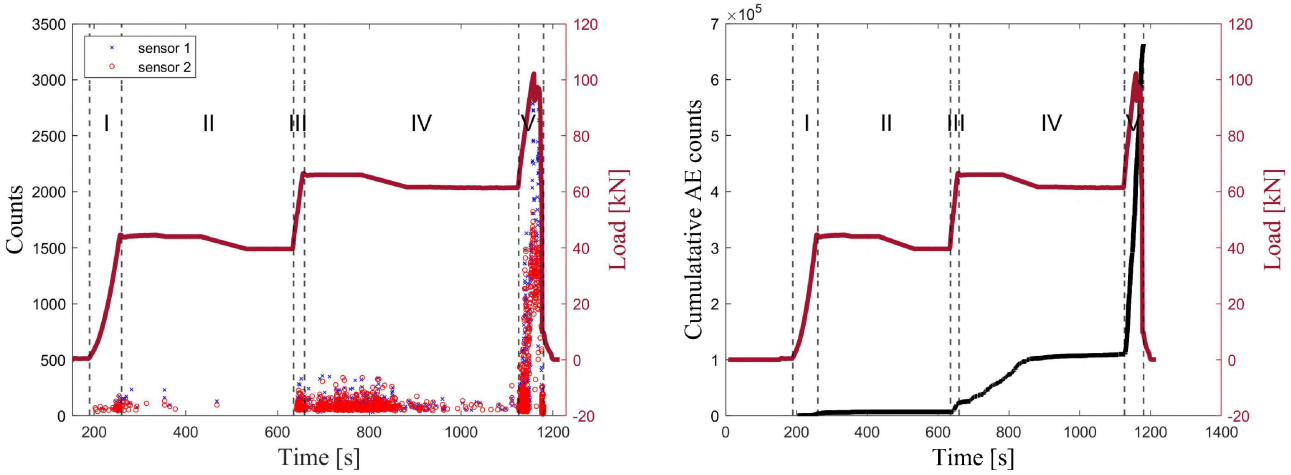


***Figure 7.*** *Left: Counts recorded by each sensor over time. Right: Cumulative counts from both sensors. The red line represents the applied load curve in the test.*

this damage initiated in stage III continues if the load remains constant; however, when the load is decreased, the cumulative AE counts stabilize, indicating that the specimen is susceptible in this part to damage around the 60% of previous peak load. Subsequently, in stage V, when the load returns to its previous maximum, the cumulative counts resume their consistent rise in accordance with the maximum applied load.

## MARSE Energy

This parameter, known as “Energy”, is defined as the measured area under the rectified AE signal envelope (MARSE), represented in voltage-time units. The left graph in Figure 8 illustrates the hit energy for channels 1 and 2 during the test. On the right graph, the accumulated energy displays a significant increase towards the end of the test, especially in the final stage when the specimen fractures near the limit of the maximum applied load. Throughout stages I and II, the AE Energy remained at a low level. It’s only after the peak load in stage III that a slight increase in energy is observed in comparison; however, in stage V, when the load decreases, the energy remains stable. Finally, as we enter the last stage, V, the energy experiences a sharp increase, reaching its maximum at the peak load moment. These abrupt changes in energy are linked, according to other studies, to fracture processes, damage, and energy dissipation within the specimen [(Du, 2020); (Ou, 2024)].

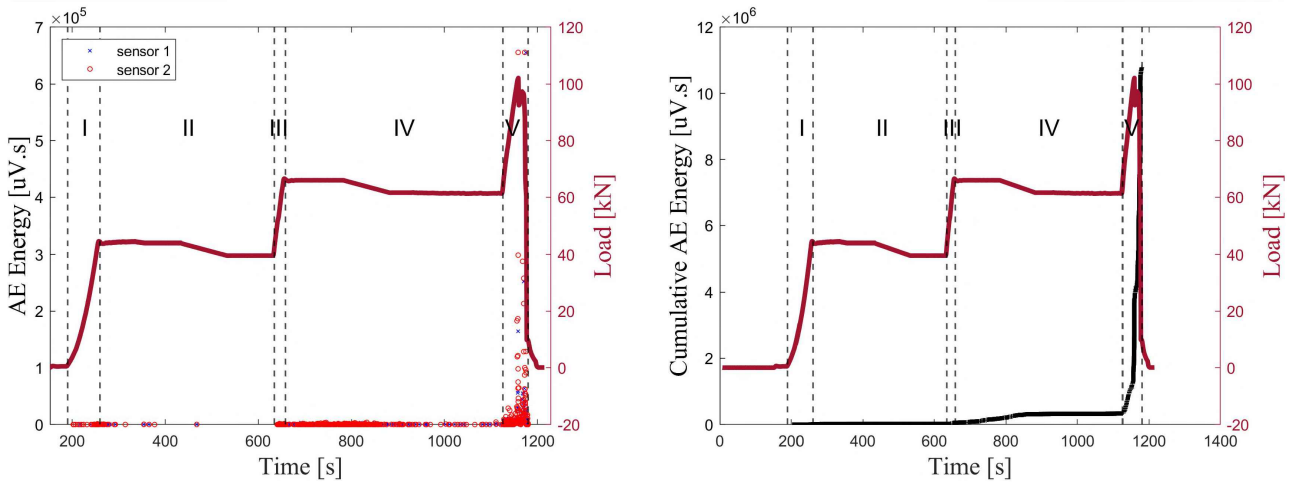


***Figure 8.*** *Left: Energy received by both channels over time. Right: Cumulative energy from all sensors over time.*

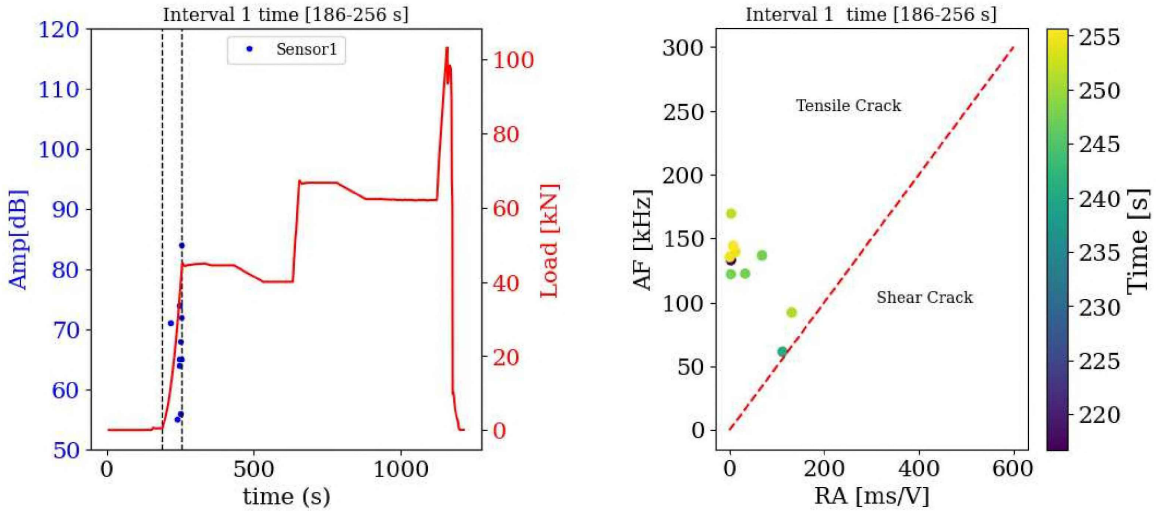


***Figure 9.*** *Left: AE events detected by sensor 1 in the time interval 186-256 s based on their amplitude. The applied load on the rock is shown in red. Right: AF vs RA, exposing the predominant fracture modes (tensile or shear).*

## Evolution tensil and shear fracture

The following are the time intervals corresponding to the different stages of the test, along with the respective analysis of the results obtained. During each interval, trends in the secondary parameters RA and AF were examined to determine the predominant fracture modes (tensile or shear). In the crack classification method based on two indices of AF value and RA value, a manual line of 45° is usually adopted to classify the tensile, shear and mixed mode cracks (Niu et al., 2020; Li et al., 2022). According to the research of Niu et al. (2020) on the classification of rock crack types, we choose the ratio of RA-AF of 2:1 as the transition line between tension and shear cracks in the next figures.

**Stage I (186-256 s) - Load increase** In this interval, a total of 41 hits were recorded, with 10 AE hits detected in channel 1 and 31 AE hits in channel 2. During this interval, the applied load on the basalt rock sample increased for the first time, reaching 40 kN. Figure 9 illustrates the maximum amplitude of the events identified in channel 1, as well as the classification of hits interms of tensile or shear fracture modes, based on the AF vs RA graph. Out of the 10 events recorded in channel 1, all events were identified as tensile events.

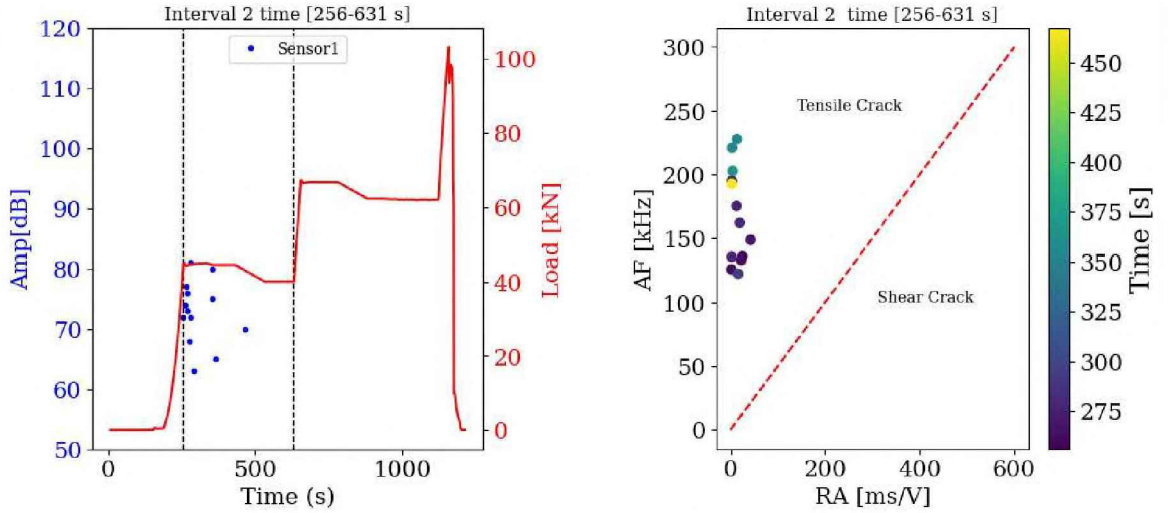


***Figure 10.*** *Left: AE events detected in the 280-623 s time interval in terms of their amplitude. The applied load on the rock is shown in red. Right: AF vs RA, illustrating the predominant fracture modes (tensile or shear).*

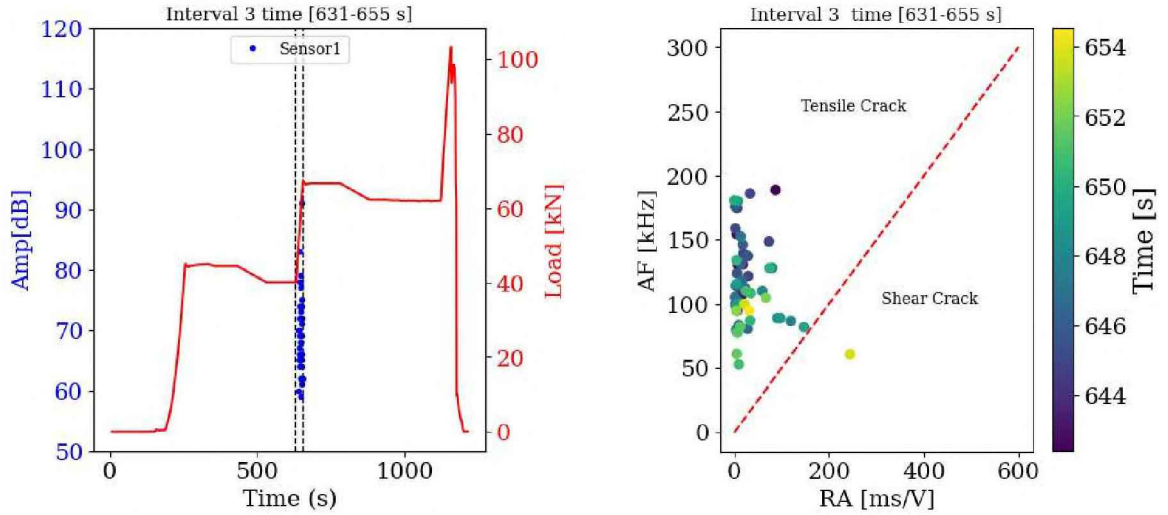


***Figure 11.*** *Left: AE events detected in the time interval 631-655 s based on their amplitude. The applied load on the rock is shown in red. Right: AF vs RA, exposing the predominant fracture modes (tensile or shear).*

**Stage II (256-631 s) - Constant load and decrease** In this interval, the load remained constant and decreased in the final part. A total of 34 hits were recorded, with 13 AE hits detected in channel 1 and 21 hits in channel 2. Figure 10 illustrates the maximum amplitude of the events identified in channel 1, as well as the classification of hits in terms of tensile or shear fracture modes, based on the AF vs RA graph. Out of the 13 hits recorded in channel 1, all 13 hits were identified as tensile events.

**Stage III (631-655 s) - Increased load** In this interval, the applied load on the basalt rock sample increased for the second time, reaching 65 kN. A total of 146 hits were identified, with 54 AE hits in channel 1 and 92 AE hits in channel 2. Figure 11 illustrates the maximum amplitude of the events detected in channel 1 and the events classified as tensile or shear fractures based on the AF vs RA graph. Out of the 54 events in channel 1, 53 were classified as tensile events, and 1 as shear events.

**Stage IV (655-1122 s) - Constant load-decreased** During this interval, the load remained constant, decreased, and then returned to a constant state in the final segment. A total of 891 events were identified between channel 1 (313 AE events) and channel 2 (578 AE events). Figure 12 shows the maximum amplitude of the events detected in channel 1 and the events classified as tensile or shear

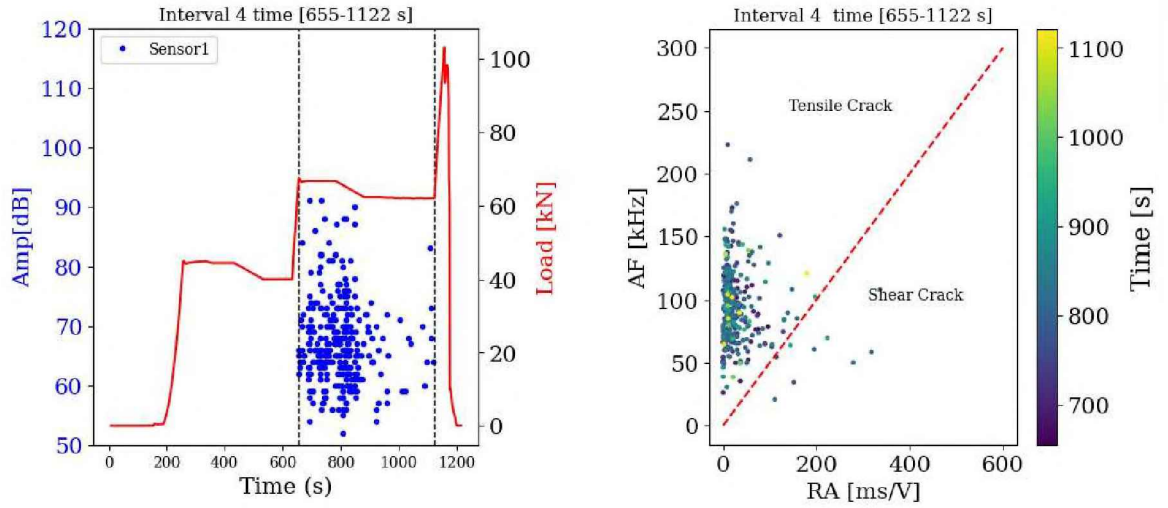


***Figure 12.*** *Left: AE events detected within the time interval of 650-1110 s as a function of their amplitude. The applied load on the rock is highlighted in red. Right: AF vs RA, illustrating the predominant fracture modes (tensile or shear).*

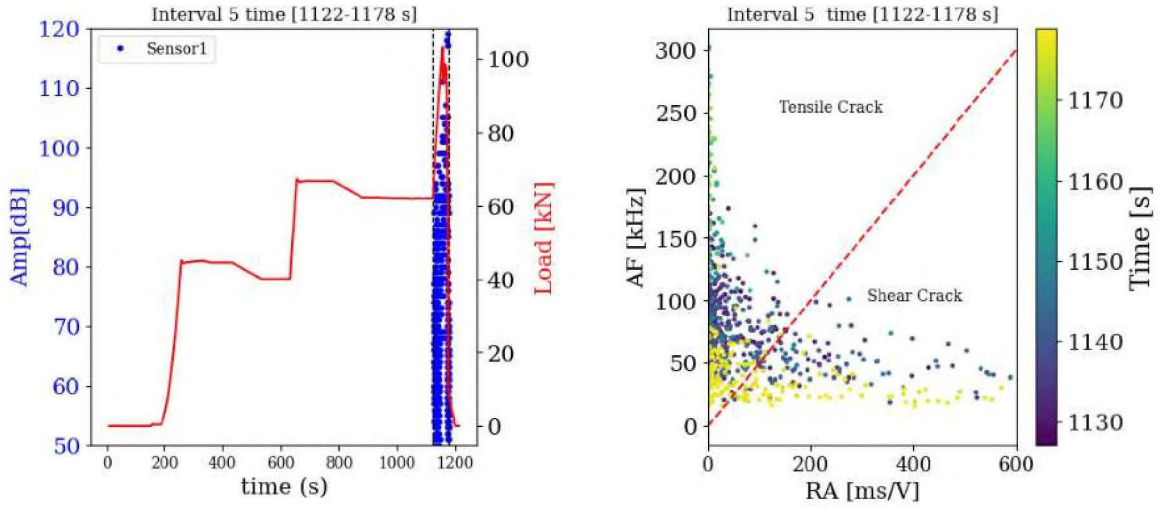


***Figure 13.*** *Left: AE events detected in the time interval 1122-1178 s based on their amplitude. The applied load on the rock is shown in red. Right: AF vs RA, exposing the predominant fracture modes (tensile or shear).*

fractures based on the AF vs RA graph. Out of the 313 events in channel 1, 304 were classified as tensile events, and 9 as shear events.

**Stage V (1122-1178s) - Increased load until rock fracture** In this stage, the applied load on the basalt rock sample increased for the third time, from 62 kN to 110 kN, resulting in the fracture of the rock. A total of 1637 events were identified between channel 1 (730 AE events) and channel 2 (907 AE events). Figure 13 shows the maximum amplitude of the events detected in channel 1 and the events classified as tensile or shear fractures based on the AF vs RA graph. Out of the 730 events in channel 1, 569 were classified as tensile events, and 171 as shear events. Towards the end of the stage (yellow color dots), there is a significant increase in shear-type events with low AF and high RA values.

### Proportion of classified cracks under different stress levels

The correlation between cumulative tensile events, cumulative shear events, and the applied load is illustrated in Figure 14. Notably, the cumulative tensile events throughout the loading process notably

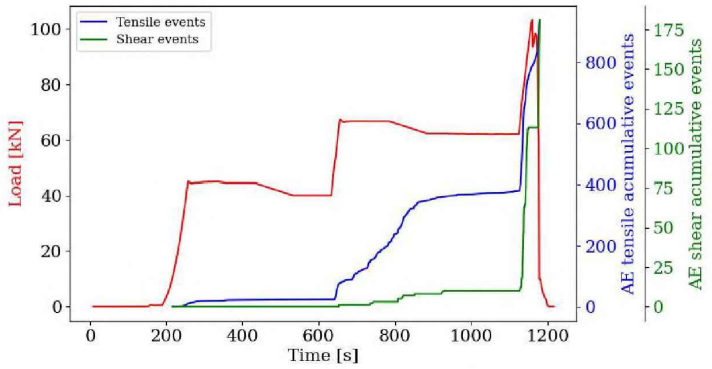


***Figure 14.*** *Accumulated AE tensile events and shear events over time.*

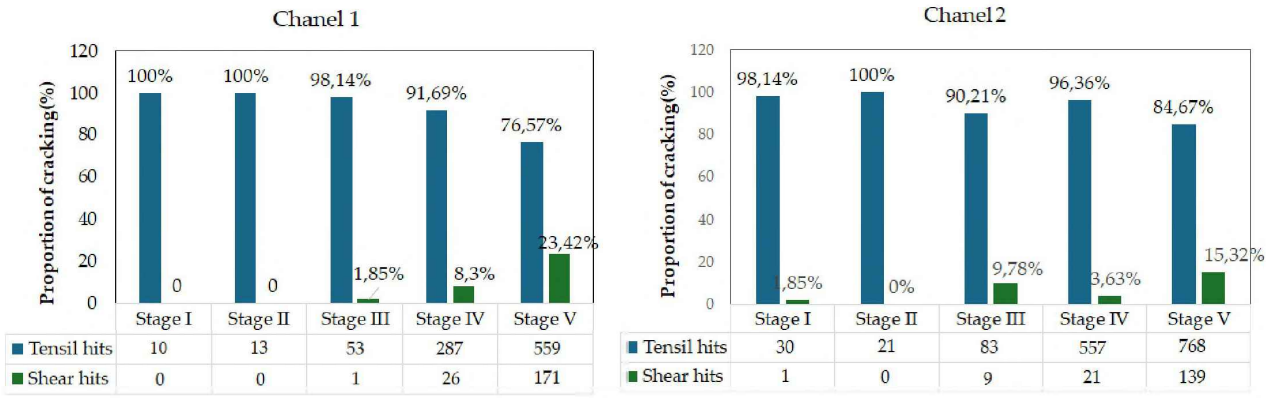


***Figure 15.*** *Proportion of cracking of tensile and shear for sensor 1 and sensor 2 in each stage.*

surpass the corresponding shear events. The progression pattern of cumulative tensile events closely mirrors that of cumulative shear events. Clearly, there is a sudden increase in the number of events near the peak stress and in the post-peak stage. Nevertheless, the overall prevalence of tensile events over shear events aligns with the macroscopic failure characteristics of the rock, as depicted in Figure 8.

Employing the previously outlined crack classification method, a thorough statistical analysis of proportion of tensile and shear events was conducted across the five stages, as illustrated in Figure 15. Upon scrutinizing the total number of events generated throughout the five stages, a clear trend emerges – most AE events manifest after the third stage ($>$ 40% load). In all instances, tensile fractures dominate; however, there is a substantial increase in shear-type fractures during the final stage.

## b-value

We've undertaken a detailed analysis by processing the peak amplitude data from 50 subsets of AE in sequential, non-overlapping time and stress windows. Several investigations have indicated that the selection of the window size does not significantly alter the overall trend of the b-value (Colombo et al., 2003; Liu et al., 2019). This approach provides a comprehensive examination of the variations in AE signals, allowing us to discern patterns and trends across distinct temporal and stress intervals. By systematically evaluating these subsets, we aim to derive valuable insights into the behavior and characteristics of acoustic emissions under varying conditions, contributing to a deeper understanding of the underlying phenomena. Considering the correlation between b value and energy, the AE energy and b value are plotted together in this section to facilitate the analysis. The characteristics of the AE energy and b value are shown in Figure 16.

In a comprehensive examination, an upward shift in the b-value serves as a distinctive indicator,

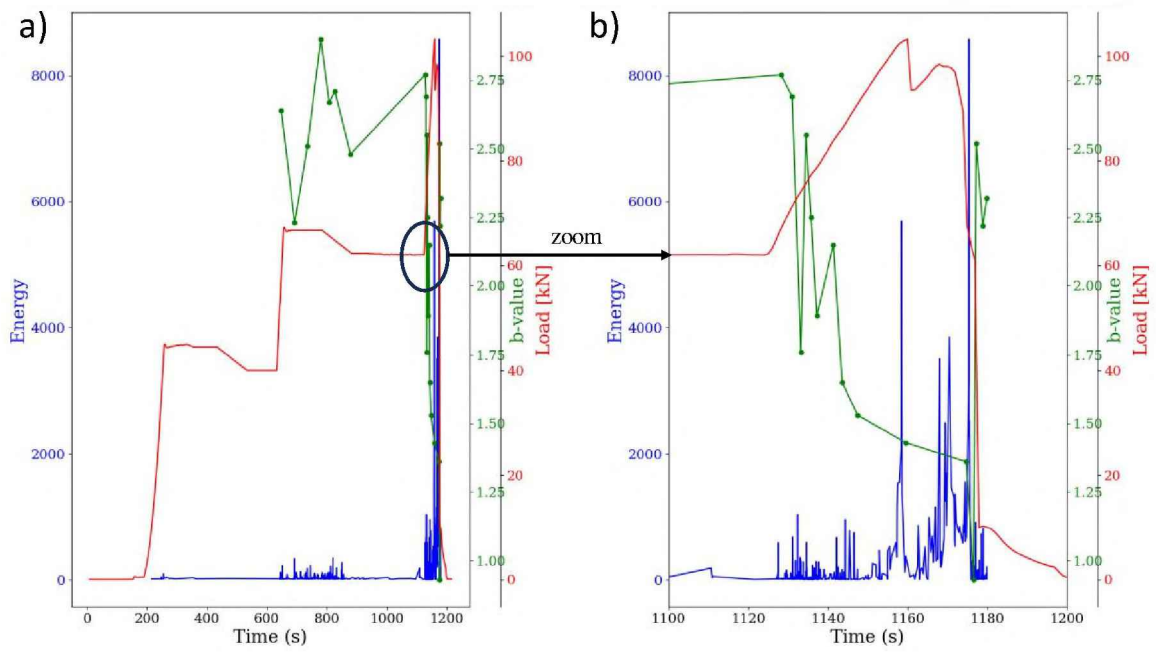


***Figure 16.*** *b-values obtained by using the Gutenberg-Richter relationship.*

denoting an increase in the frequency of small-scale events and underscoring the prevalence of such fractures within rock materials. This elevation in the b-value implies a dynamic state where smaller fractures play a more prominent role in the overall fracture process. Subsequently, when the b-value stabilizes, it signifies a harmonious balance between large-scale and small-scale events. This stabilization indicates a phase of steady expansion in the fracture state of rock materials, where both larger and smaller fractures coexist in a relatively proportionate manner.

Conversely, a decrease in the b-value introduces a contrasting scenario, implying a shift towards an increasing proportion of large-scale events. This reduction in the b-value suggests the growing dominance of larger fractures within the rock materials, potentially influencing the overall stability and integrity of the rock matrix. These variations in the b-value offer valuable insights into the evolving dynamics of rock fractures, providing a nuanced understanding of the underlying mechanisms influencing rock behavior under different stress conditions (Rao & Lakshmi, 2006; Xie et al., 2023).

The abrupt increase in acoustic emission (AE) energy corresponds to a sudden decrease in the b-value in Figure 16. The early loading stage is characterized by a relatively low number of AE events, and a prolonged period features the absence of an AE b-value. The high AE b-value in the initial loading stage (I, II and III) is linked to the limited load applied and the development of small-scale cracks in rock materials. As the load approaches its peak (stage IV), the expansion of large-scale cracks in the rock results in a sudden increase in AE energy, accompanied by a decrease in the AE b-value. This sudden energy surge aligns consistently with the decline in the AE b-value. b-value variations and AE energy offers insights into the evolving fracture dynamics of rock materials during different loading stages.

## DISCUSSION

The test comprised five distinct load stages, as illustrated in Figures 7 and 8. The initial phase, referred to as the quiet stage (Stage I), corresponds to the early loading period with relatively low stress levels. During this phase, the AE event rate in rocks under different stress states remains at a low level, and the cumulative AE events exhibit a relatively flat growth. This subdued activity is attributed to the AE signals generated primarily by the closed compaction of primary defects such as pores and fractures

in the rock, resulting in a limited number of AE signals.

Transitioning to Stage II, where the load remains constant and decreases, a few events are observed. With further stress escalation in Stage III up to 66 kN of applied load, the AE event rate experiences a pronounced increase, indicating the onset of rapid growth. At this stage, the sample undergoes damage. Although the load remains constant at 65 kN in the initial part of Stage IV, the AE event rate increases due to microfracturing incurred in Stage III. In the latter part of Stage IV, as the applied load decreases from 65 kN to 61 kN, the AE rate decreases significantly until it ceases emitting altogether.

In Stage V, the load increases again and surpasses 61 kN. It is observed that the AE rate increases abruptly, reaching its peak value near the maximum applied load. This surge is attributed to crack expansion, connection, and mutual penetration within the rock.

The b-value also exhibits significant changes throughout the fracture process. In the initial stages of the fracture process (I, II, III), the b-value varied from 2.5, displaying temporal fluctuations between 2.25 and 2.75 in the IV stage. Subsequently, it decreased with an increase in load, reaching a minimum value of 1.5 at the peak load, and further descended to 1.0 thereafter. All these changes align with the peak energy values in the corresponding stages.

For the tested basalt specimens, cracking events characterized by low RA (mainly ranging from 20 to 50 ms/v) and high AF values (mainly distributed from 40 to 300 kHz) suggest a tensile cracking mode. Conversely, cracking events featuring high RA (mainly ranging from 50 to 600 ms/v) and low AF values (mostly distributed from 25 to 50 kHz) indicate a triggered shear cracking mode. Tensile fracture modes dominate throughout the process, but gradually, From the third stage onward, there is a progressive increase in shear cracking, leading to a considerable rise of shear cracks in the final stage.

Furthermore, while AE signals provide valuable information about the internal deformation and damage evolution of the rocks, they may not fully capture all aspects of the fracture process. Other complementary techniques, such as microscopy or mechanical testing, could provide additional insights into the underlying mechanisms of rock failure.

Despite these limitations, this study contributes to our understanding of rock fracture processes and provides a basis for further research in this field. By recognizing these constraints, future studies can refine experimental methodologies and expand the scope of investigation to enhance our understanding of rock mechanics and engineering applications.

## CONCLUSIONS

A uniaxial compression test was conducted on various basaltic rocks until failure. This study provides added value as it examines the fracture process under different loading conditions. Constant loading between each positive slope loading step was performed to check the damage evolution for different stress levels. The basalt samples fractured near the maximum applied load, approximately at 100 kN.

AE signals were detected, and the most representative parameters for evaluating damage were Amplitude, Cumulative Hits, Counts, and Energy. The highest Acoustic Emission (AE) rate is observed in the final loading stage (V), beyond a value of 61 kN of the maximum applied load, leading the material from microfracture to collapse. This is associated with the increasing damage initiated in stage III, observed in stage IV by the emission of elastic waves under constant load. A decrease in the AE event rate is noticeable when the load remains constant.

The predominant fracture mode is determined by analyzing the AF-RA scatter plot, and the evolving characteristics of tensile and shear events during the loading process are examined. In stages I, II, and III, most AF-RA points were situated in the upper part of the plot, indicating a predominantly tensile mode during these stages. However, after stage III and nearing the peak load, there was a

considerable increase in the proportion of shear events.

In this study, AE b-values were calculated for each set of 50 hits amplitudes over time. The analysis of AE, particularly in terms of b-values, conducted at stress levels approaching failure, distinctly revealed the initiation of unstable cracking and the subsequent coalescence of cracks leading to the dynamic failure of the tested rock. These findings hold crucial implications for monitoring the stability and integrity of rock formations across various scales. The AE b value under different stress states share a similar law. At the initial stage of loading, the AE b value is high, load is close to the peak range, AE energy increases significantly, and the b value decreases significantly before dropping to the lowest point before the peak. The lowest point of the b value exhibits a good correspondence to the point of sudden increase in AE energy.

Analyzing the load descent stages not only showed crucial moments of increased rock damage but also offered detailed insights into the changing fracture dynamics. After the initial load ascent, the second stage indicated a lack of acoustic emission events, suggesting a relatively stable condition. However, in the third stage, as the load reached around 60% of its maximum, the specimen experienced significant damage, continually microfracturing during the subsequent constant load stage. In the final stage, nearing the peak load, a noticeable decrease in the b-value and a simultaneous substantial increase in AE energy indicated a consistent expansion of cracks within the rock. This multi-stage observation highlights the complex relationship between load descent, acoustic emission events, and changes in the b-value, providing valuable insights into the progressive failure mechanisms of the tested rock specimen.

## REFERENCES

**Calabrese, L. & Proverbio, E.** (2020). A review on the applications of acoustic emission technique in the study of stress corrosion cracking. *Corrosion and Materials Degradation*, 2(1), 1–30.

**Cao, K., Xu, Y., Khan, N. M., Li, X., Cui, R., Hussain, S., & Alarifi, S. S.** (2023). A comprehensive model for evaluating infrared radiation and acoustic emission characteristics of sandstone fracture. *Engineering Fracture Mechanics*, 283, 109217.

**Carrasco, A., Méndez, F., Leaman, F., & Molina Vicuña, C.** (2021). Short review of the use of acoustic emissions for detection and monitoring of cracks. *Acoustics Australia*, 49, 273–280.

**Casals, B., Dahmen, K. A., Gou, B., Rooke, S., & Salje, E. K.** (2021). The duration-energy-size enigma for acoustic emission. *Scientific Reports*, 11(1), 5590.

**Colombo, I. S., Main, I. G., & Forde, M. C.** (2003). Assessing damage of reinforced concrete beam using "b-value" analysis of acoustic emission signals. *Journal of Materials in Civil Engineering*, 15(3), 280–286.

**Dong, L., Chen, Y., Sun, D., Zhang, Y., & Deng, S.** (2023). Implications for identification of principal stress directions from acoustic emission characteristics of granite under biaxial compression experiments. *Journal of Rock Mechanics and Geotechnical Engineering*, 15(4), 852–863.

**Filipussi, D. A.** (2018). Caracterización de daño por "b-value" de eventos de emisión acústica en ensayos de rotura de roca andesita. *Matéria (Rio de Janeiro)*, 23, e12068.

**Li, S., Yang, D., Huang, Z., Gu, Q., & Zhao, K.** (2022). Acoustic emission characteristics and failure mode analysis of rock failure under complex stress state. *Theoretical and Applied Fracture Mechanics*, 122, 103666.

**Liu, X. L., Liu, Z., Li, X. B., & Han, M. S.** (2019). Acoustic emission b-values of limestone under uniaxial compression and brazilian splitting loads. *Rock and Soil Mechanics*, 40(S1), 267–274.

**Niu, Y., Hu, Y. J., & Wang, J. G.** (2023). Cracking characteristics and damage assessment of filled rocks using acoustic emission technology. *International Journal of Geomechanics*, 23(4), 04023013.

**Niu, Y., Zhou, X. P., & Berto, F.** (2020). Evaluation of fracture mode classification in flawed red sandstone under uniaxial compression. *Theoretical and Applied Fracture Mechanics*, 107, 102528.

**Ono, K.** (2011). Acoustic emission in materials research-a review. *Journal of Acoustic Emission*, 29.

**Rao, M. V. M. S. & Lakshmi, K. J.** (2006). Amplitude distribution analysis of acoustic emissions and investigation of the development of brittle fracture in rock. *Unpublished*.

**Rodríguez, P. & Celestino, T. B.** (2019). Application of acoustic emission monitoring and signal analysis to the qualitative and quantitative characterization of the fracturing process in rocks. *Engineering Fracture Mechanics*, 210, 54–69.

**Shi, X., Xu, H., Che, M., Xiao, C., Ni, H., & Gao, Q.** (2023). Investigations of fracture behavior and pore structure change in pulse fracturing for cement block. *International Journal of Rock Mechanics and Mining Sciences*, 166, 105366.

**Wang, Q., Chen, J., Guo, J., Luo, Y., Wang, H., & Liu, Q.** (2019). Acoustic emission characteristics and energy mechanism in karst limestone failure under uniaxial and triaxial compression. *Bulletin of Engineering Geology and the Environment*, 78, 1427–1442.

**Wieser, C., Käsling, H., Raith, M., Richter, R., Moser, D., Gemander, F., & Thuro, K.** (2015). Acoustic emission technique to detect micro cracking during uniaxial compression of brittle rocks. *Engineering Geology for Society and Territory-Volume 6: Applied Geology for Major Engineering Projects*, 465–468. Springer International Publishing.

**Wu, S., Qin, G., & Cao, J.** (2022). Deformation, failure, and acoustic emission characteristics under different lithological confining pressures. *Materials*, 15(12), 4257.

**Xie, Y., Hou, M. Z., & Li, C.** (2023). Anisotropic characteristics of acoustic emission and the corresponding multifractal spectrum during progressive failure of shale under cyclic loading. *International Journal of Rock Mechanics and Mining Sciences*, 165, 105364.

**Zhang, Z., Liu, X., Zhang, Y., Qin, X., & Khan, M.** (2021). Comparative study on fracture characteristics of coal and rock samples based on acoustic emission technology. *Theoretical and Applied Fracture Mechanics*, 111, 102851.

**Zhao, S., Chao, Q., Yang, L., Qin, K., & Zuo, J.** (2022). A review on application of acoustic emission in coal—analysis based on citespace knowledge network. *Processes*, 10(11), 2397.